



# Degradation pathway and kinetics of 1-alkyl-3-methylimidazolium bromides oxidation in an ultrasonic nanoscale zero-valent iron/hydrogen peroxide system

Haimei Zhou<sup>a</sup>, Yuanyuan Shen<sup>a</sup>, Ping Lv<sup>a</sup>, Jianji Wang<sup>b,\*</sup>, Pu Li<sup>a</sup>

<sup>a</sup> Faculty of Forensic Medicine, Henan University of Science and Technology, Luoyang, Henan 471003, PR China

<sup>b</sup> School of Chemistry and Chemical Engineering, Key Laboratory of Green Chemical Media and Reactions, Ministry of Education, Henan Normal University, Xinxiang, Henan 453007, PR China

## HIGHLIGHTS

- Degradation of five methylimidazolium ionic liquids (ILs) was studied.
- Degradation of the ILs can be described by the second order kinetic model.
- A number of intermediates were identified and the degradation pathways were suggested.
- Ultrasonic nanoscale zero-valent iron/H<sub>2</sub>O<sub>2</sub> is effective for the ILs degradation.

## ARTICLE INFO

### Article history:

Received 14 May 2014

Received in revised form 18 October 2014

Accepted 23 October 2014

Available online 11 November 2014

### Keywords:

Ionic liquid

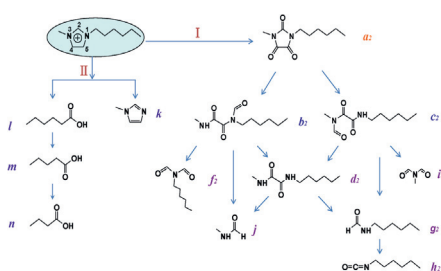
Degradation pathway

Nanoscale zero-valent iron

Hydrogen peroxide

Ultrasound

## GRAPHICAL ABSTRACT



## ABSTRACT

Fenton and Fenton-like oxidation has been already demonstrated to be efficient for the degradation of imidazolium ionic liquids (ILs), but little is known for their degradation pathway and kinetics in such systems. In this work, degradation pathway and kinetics of 1-alkyl-3-methylimidazolium bromides ([C<sub>n</sub>mim]Br, n = 2, 4, 6, 8, and 10) were investigated in an ultrasound nanoscale zero-valent iron/hydrogen peroxide (US-nZVI/H<sub>2</sub>O<sub>2</sub>) system. For this purpose, 1-butyl-3-methylimidazolium bromide ([C<sub>4</sub>mim]Br) was used as a representative ionic liquid to optimize pH value, nZVI dose, and H<sub>2</sub>O<sub>2</sub> concentration for the degradation reaction. Then, the degradation kinetics of [C<sub>n</sub>mim]Br was investigated under optimal conditions, and their degradation intermediates were monitored by gas chromatography-mass spectrometry (GC-MS). It was shown that the degradation of [C<sub>n</sub>mim]Br in such a heterogeneous Fenton-like system could be described by a second order kinetic model, and a number of intermediate products were detected. Based on these intermediate products, detailed pathways were proposed for the degradation of [C<sub>n</sub>mim]Br in the ultrasound-assisted nZVI/H<sub>2</sub>O<sub>2</sub> system. These findings may be useful for the better understanding of degradation mechanism of the imidazolium ILs in aqueous solutions.

© 2014 Elsevier B.V. All rights reserved.

## 1. Introduction

Ionic liquids (ILs) are usually composed of an inorganic or organic anion and an asymmetric bulky organic cation like alkylimidazolium, alkylpyridinium, alkylpyrrolidinium, morpholinium, or piperidinium. Due to the unique physical and chemical properties such as extremely low vapor pressure, wide liquid-state

\* Corresponding author. Tel.: +86 373 3325805; fax: +86 373 3326445.  
E-mail address: [jwang@henannu.edu.cn](mailto:jwang@henannu.edu.cn) (J. Wang).

temperature range, and good thermal and chemical stability, ILs are considered as a new class of environmental-friendly solvents following supercritical fluids and aqueous two-phase systems, and show a good prospect in synthesis chemistry, catalysis reactions, electrochemistry, separation, and purification science [1–3]. However, with the development of ILs, scientists gradually realized that the green characteristic of ILs is controversial. It has been found that most of the ILs reported up to now is toxic and corrosive, and ecotoxicity of some ILs is even higher than that of traditional organic solvents [4–6]. Consequently, study on the removal of ILs from aqueous solutions is of great significance.

Current studies have shown that the majority of ILs, especially the most commonly used imidazolium salts, was stable and highly resistant to biodegradation [7–11]. By contrast, chemical degradation can offer an efficient way to conquer the chemical and thermal stability of ILs. In recent years, therefore, advanced oxidation methods have been used for the degradation of ILs, such as UV irradiation, UV/H<sub>2</sub>O<sub>2</sub>, UV/TiO<sub>2</sub> [12], ultrasound-H<sub>2</sub>O<sub>2</sub>/CH<sub>3</sub>COOH [13], Fenton and Fenton-like reagent [14–17] and so on. Among these methods, Fenton and Fenton-like processes are believed to be efficient and reliable for the degradation of ILs.

Fenton oxidation using hydrogen peroxide as oxidant and iron salts as catalyst can result in the generation of hydroxyl radicals ( $\cdot\text{OH}$ ), which are powerful but relatively non selective oxidizing agent and can oxidize many organic contaminants rapidly [18,19]. Fenton reaction is usually modified for environmental application [14–16,20], and the modified Fenton reaction (Fenton-like reaction) is more vigorous than the standard Fenton system.

The use of homogeneous Fenton-like processes (H<sub>2</sub>O<sub>2</sub>/Fe<sup>3+</sup>) was studied by Siedlecka et al. [15–17,21] for the degradation of 1-butyl-3-methylimidazolium chloride ([C<sub>4</sub>mim]Cl), 1-butyl-3-methylimidazolium trifluoromethanesulfonate ([C<sub>4</sub>mim][CF<sub>3</sub>SO<sub>3</sub>]), 1-butyl-3-methylimidazolium tricyanmethide ([C<sub>4</sub>mim][C(CN)<sub>3</sub>], 1-hexyl-3-methylimidazolium chloride ([C<sub>6</sub>mim]Cl), and 1-octyl-3-methylimidazolium chloride ([C<sub>8</sub>mim]Cl) in water. It was found that the reaction rate for [C<sub>n</sub>mim]<sup>+</sup> degradation was influenced by the anions in the order: Cl<sup>-</sup> > C(CN)<sub>3</sub><sup>-</sup> > CF<sub>3</sub>SO<sub>3</sub><sup>-</sup>, and by using 1 mmol L<sup>-1</sup> of Fe(III) and 100 mmol L<sup>-1</sup> of H<sub>2</sub>O<sub>2</sub>, the degradation efficiency was 97%, 88%, and 68%, respectively, for [C<sub>4</sub>mim]Cl, [C<sub>6</sub>mim]Cl, and [C<sub>8</sub>mim]Cl during 90 min of degradation reaction. Investigations of the degradation process revealed that the oxidation rate of the imidazolium ILs by  $\cdot\text{OH}$  was structure related, and the level of degradation was dependent on the alkyl chain length. Despite the high degradation efficiency reported in the literatures, it is surprising to find that degradation pathway and kinetics of ILs are poorly understood in Fenton and Fenton-like systems.

In addition, although these processes have been effective in degradation of environmental pollutants, a large amounts of sludge-containing iron has to be produced, which weakens their applications [22–24]. To overcome the disadvantages of homogeneous Fenton and Fenton-like processes, and to consider also the possibility of catalyst recovery, heterogeneous Fenton-like systems using iron supported catalysts have been developed [23–26]. It was shown that zero-valent iron and hydrogen peroxide (ZVI/H<sub>2</sub>O<sub>2</sub>) could be considered as an effective alternative system for the treatment of some organic pollutants. In the heterogeneous system of ZVI/H<sub>2</sub>O<sub>2</sub>, ZVI can induce the Fenton reaction as follows:



In acidic condition, the surface of ZVI is easy to be corroded to generate Fe<sup>2+</sup> and hydrogen gas (Eq. (1)), and the Fe<sup>3+</sup> produced in this system (Eq. (2)) can be reduced into Fe<sup>2+</sup> by zero-valent

iron metal (Eq. (3)). The reagents used in ZVI/H<sub>2</sub>O<sub>2</sub> heterogeneous system are safe to handle and the process is environmentally benign [23,25].

It is reported that nanoscale zero-valent iron (nZVI) exhibits greater reactivity than micro-sized particles of ZVI. Because of its large surface area and low diffusion resistance, nZVI is more efficient for the acceleration of Fenton-like reactions than the conventional heterogeneous catalysts [27–29]. Under acidic conditions, nZVI together with H<sub>2</sub>O<sub>2</sub> is able to produce reactive species similar to those in Fenton system, and to form a heterogeneous Fenton-like system. Additionally, it is well known that ultrasound (US) is a form of energy and can be used to generate cavitation microbubbles and radical reactions. Introduction of US can significantly improve pollutants degradation in Fenton and Fenton-like reaction systems [30,31]. Therefore, it is expected that the degradation of IL wastewater would be effective in an ultrasound-assisted nZVI/H<sub>2</sub>O<sub>2</sub> system.

In this work, we focus our attention on the degradation pathway and kinetics of the commonly used imidazolium ILs in ultrasound nanoscale zero-valent iron/hydrogen peroxide (US-nZVI/H<sub>2</sub>O<sub>2</sub>) systems. Here, the ILs of 1-alkyl-3-methylimidazolium bromides ([C<sub>n</sub>mim]Br, *n*=2, 4, 6, 8, and 10) have been chosen for the degradation investigations. This consideration makes it possible to examine the effects of alkyl chain length on the degradation pathway and kinetics of such ILs in aqueous solutions. From a detailed kinetic and degradation intermediate study, important results have been found for the understanding of imidazolium ILs degradation.

## 2. Materials and methods

### 2.1. Chemicals and reagents

The ILs used in this work were as follows: 1-ethyl-3-methylimidazolium bromide ([C<sub>2</sub>mim]Br), 1-butyl-3-methylimidazolium bromide ([C<sub>4</sub>mim]Br), 1-hexyl-3-methylimidazolium bromide ([C<sub>6</sub>mim]Br), 1-octyl-3-methylimidazolium bromide ([C<sub>8</sub>mim]Br), and 1-decyl-3-methylimidazolium bromide ([C<sub>10</sub>mim]Br). All the ILs (purity >99%) were provided by Key Laboratory of Green Chemical Media and Reactions, Henan Normal University, and used without further purification. Stock solutions of [C<sub>n</sub>mim]Br (25 mmol L<sup>-1</sup>) were prepared in water purified from a Milli-Q apparatus (Millipore, Co., USA) and then stored at 4 °C.

nZVI powders (polycrystalline nano-iron with a face-centered cubic structure, purity 99%) with a claimed average particle size of around 20 nm were purchased from Qinhuangdao Taiji Ring Nano Products Co., Ltd. (Qinhuangdao, China). The nZVI was characterized with an environmental scanning electron microscope (ESEM, Quanta 650 FEG, FEI, USA) and an energy dispersive X-ray spectrometer (EDX, Genesis Apex 2, EDAX, USA). Reductive iron powder of zero-valent iron (99%, 325 mesh) was from Beijing Chemical Reagent Co., Ltd. (Beijing, China), and 30% hydrogen peroxide was from Haohua Chemical Reagent Co., Ltd. (Luoyang, China). Methanol and acetonitrile (LC grade) were from Kernal Chemical Reagent Development Center (Tianjin, China). Ethyl acetate, benzene, ether, potassium dihydrogen phosphate, and triethylamine (analytical reagent grade) were acquired from Beijing Chemical Factory (Beijing, China).

### 2.2. Degradation experiments

All the degradation experiments were conducted in a flask (50 mL) placed in a KQ-300GVDV ultrasonic cleaner (300 W, 45 kHz, or 80 kHz, Kunshan Ultrasonic Instrument Co., Ltd., China).

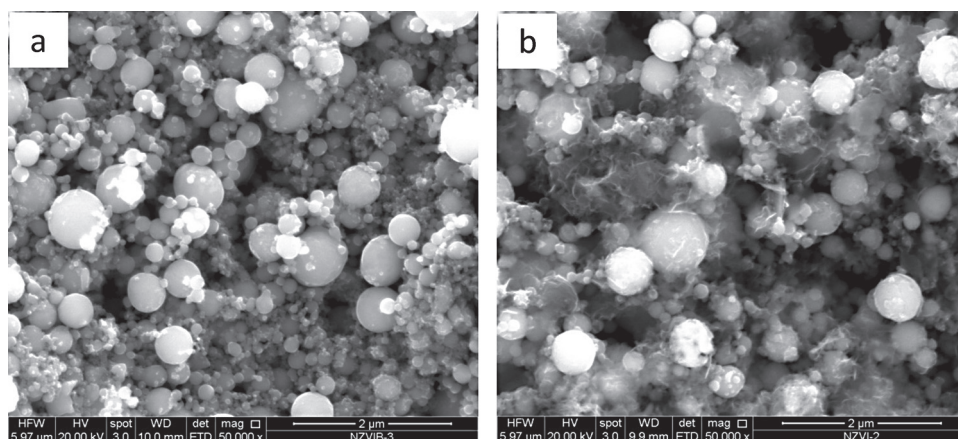


Fig. 1. SEM micrographs of the nZVI: (a), before reaction; and (b), after 120 min reaction.

When ultrasonic irradiation was not employed, the degradation experiments were carried out in a commonly used temperature controlling apparatus with a magnetic stirrer. Reaction mixture was prepared by the addition of 25 mL of  $[C_n\text{mim}]\text{Br}$  sample ( $2.0\text{ mmol L}^{-1}$ ) and appropriate quantity of nZVI particles in the flask, and the pH of the mixture was adjusted to 3.0. The reaction was started with the addition of a given amount of  $\text{H}_2\text{O}_2$ . Samples were collected from the flask by a  $0.45\text{-}\mu\text{m}$ -pore-size membrane syringe filter (Shanghai Anpel Scientific Instrument Co., Ltd.) after various reaction times, and immediately quenched with 0.2 mL of methanol. The degradation reaction was carried out at  $30^\circ\text{C}$  and stopped at the reaction time of 120 min.

### 2.3. Analytical procedures

#### 2.3.1. HPLC analysis

The concentrations of  $[C_n\text{mim}]\text{Br}$  and hydrogen peroxide were determined by means of a high-performance liquid chromatography (HPLC, Waters Series 1525, USA) equipped with a Symmetry C-18 column ( $150 \times 4.6\text{ mm}$ ,  $5\text{ }\mu\text{m}$ ) and an UV/VIS variable wavelength detector at 212 nm, and the column temperature was maintained at  $30^\circ\text{C}$ . Samples were analyzed at a flow rate of  $0.8\text{ mL min}^{-1}$  and the injection volume was  $10\text{ }\mu\text{L}$ . The mixture of methanol (35%, v/v) with  $25\text{ mmol L}^{-1}$  of phosphate buffer ( $\text{KH}_2\text{PO}_4/\text{H}_3\text{PO}_4$ ) in 0.5% triethylamine (pH 3.0) was used as the mobile phase for the analysis of  $[C_n\text{mim}]\text{Br}$  ( $n=2, 4, \text{ and } 6$ ) and hydrogen peroxide, while the mixture of acetonitrile (35%, v/v) with  $25\text{ mmol L}^{-1}$  of phosphate buffer ( $\text{KH}_2\text{PO}_4/\text{H}_3\text{PO}_4$ ) in 0.5% triethylamine (pH 3.0) was used as the mobile phase for the analysis of  $[C_8\text{mim}]\text{Br}$  and  $[C_{10}\text{mim}]\text{Br}$  [32]. Each sample was measured in triplicate, and then the average value was given.

#### 2.3.2. GC-MS analysis

The mixture of degradation reaction was extracted with a mixed solvent of benzene/ethyl acetate/ether (2:2:1) and analyzed by GC-MS (Agilent 6890/5973N series, USA) for the identification of degradation products of  $[C_n\text{mim}]\text{Br}$ . The optimal detection conditions are as follows: Agilent capillary column, HP-5 ms ( $30\text{ m} \times 0.25\text{ mm} \times 0.25\text{ }\mu\text{m}$ ); carrier gas, He ( $1.0\text{ mL min}^{-1}$ ); temperature program, column oven temperature,  $43^\circ\text{C}$ ; heating rate,  $10^\circ\text{C min}^{-1}$ ; final temperature,  $250^\circ\text{C}$ ; injection temperature,  $250^\circ\text{C}$ ; injection mode, splitless; injected sample volume,  $2\text{ }\mu\text{L}$ ; MS detector, ionization mode, EI (70 eV); ion source temperature,  $230^\circ\text{C}$ ; interface temperature,  $270^\circ\text{C}$ ; scan mode, full scan ( $14\text{ m/z}$ – $310\text{ m/z}$ ).

## 3. Results and discussion

### 3.1. Characterization of the nZVI

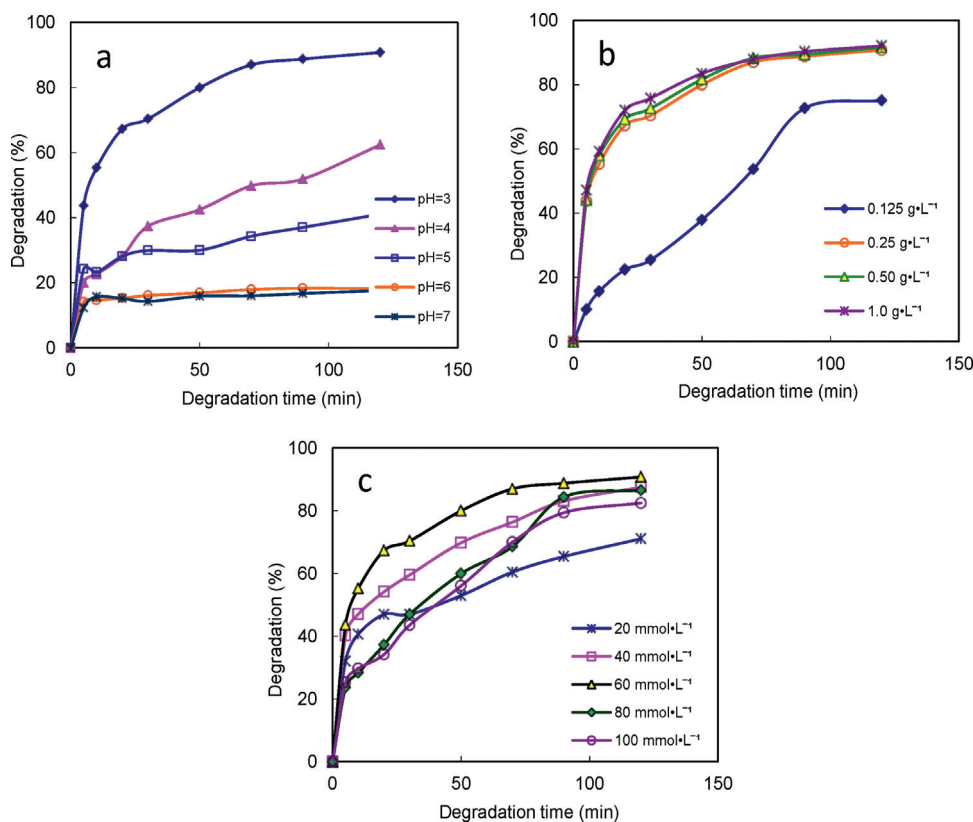
Surface morphology and composition of the nZVI particles were investigated by SEM-EDX before and after the heterogeneous Fenton-like reaction. As shown in Fig. 1a, the nanoscale iron was composed of spherical particles, and most of them had diameters in the range of 10–120 nm. After 120 min reaction, a flake-like structure was observed and most of the particles surface was covered with a certain scale cluster (Fig. 1b). EDX results showed that before the reaction, element composition of the iron particles was 98.6 wt% of iron and 1.4 wt% of oxygen, whereas 95.7 wt% of iron and 4.3 wt% of oxygen were observed after the reaction. This demonstrated that the original iron surface was oxygenated at a very small scale, and after the reaction iron oxide layer was formed by adopting a certain amount of oxygen on the nZVI surface. Although we could not identify the iron oxide species, previous studies reported that in the presence of oxygen, lepidocrocite ( $\gamma\text{-FeOOH}$ ) with a flake-like structure was formed as the first iron corrosion product [25,29,33].

### 3.2. Effect of operational parameters on the degradation of $[C_4\text{mim}]\text{Br}$

Here,  $[C_4\text{mim}]\text{Br}$  was used as a model IL to optimize the degradation reaction conditions of the ILs at  $30^\circ\text{C}$ , such as initial pH value, nZVI dosage and  $\text{H}_2\text{O}_2$  concentration.

#### 3.2.1. Effect of pH value

It has been proved that solution pH value is one of the important factors influencing the Fenton-like process in the removal of organic pollutants. Thus, the influence of initial solution pH value on the degradation efficiency of  $[C_4\text{mim}]\text{Br}$  by nZVI/ $\text{H}_2\text{O}_2$  was investigated at five different pH values of 3.0, 4.0, 5.0, 6.0, and 7.0. The result depicted in Fig. 2a showed that degradation efficiency of  $[C_4\text{mim}]\text{Br}$  increased with the decrease of solution pH value, and the best degradation degree (90.8%) was achieved at pH 3.0 within 120 min reaction. This trend is in agreement with previous reports for heterogeneous Fenton-like system: acidic condition is conducive to the increase of  $\text{Fe}^{2+}$  concentration and the generation of OH radical (Eqs. (1) and (2)) during ultrasonic irradiation [30,31]. The decreased degradation efficiency at higher pH values can be ascribed to the decomposition of  $\text{H}_2\text{O}_2$ , the lower oxidation potential of OH radical, and the deactivation of the catalyst with the formation of  $\text{Fe}^{3+}$ -hydroxo complexes in the solution, which greatly prevents the production of OH radical [15,23,24].



**Fig. 2.** Effect of operating parameters on the degradation of [C<sub>4</sub>mim]Br in US-nZVI/H<sub>2</sub>O<sub>2</sub> system at 30 °C: (a), pH; (b), nZVI dosage; (c), H<sub>2</sub>O<sub>2</sub> concentration. The other parameters were fixed at [IL] = 2.0 mmol L<sup>-1</sup>, [nZVI] = 0.25 g L<sup>-1</sup>, [H<sub>2</sub>O<sub>2</sub>] = 60 mmol L<sup>-1</sup>, pH 3.0 and ultrasound frequency = 45 kHz.

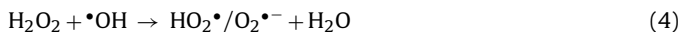
### 3.2.2. Effect of nZVI dosage

To clarify the effect of nZVI dosage on the degradation of [C<sub>4</sub>mim]Br, the measurements were carried out at pH 3.0, 60 mmol L<sup>-1</sup> of H<sub>2</sub>O<sub>2</sub> and four initial concentrations of nZVI: 0.125, 0.25, 0.50, and 1.0 (g L<sup>-1</sup>). It can be seen from Fig. 2b that at a given reaction time, degradation efficiency increased with the increase of nZVI content. When nZVI content was increased from 0.125 to 0.25 g L<sup>-1</sup>, the degradation efficiency of [C<sub>4</sub>mim]Br at 120 min increased from 75.1% to 90.8%. This is owing to the increased fresh surface of iron available for H<sub>2</sub>O<sub>2</sub> decomposition, which led to the production of more reactive oxidants such as •OH [29]. As nZVI dose was increased to 0.50 g L<sup>-1</sup> and 1.0 g L<sup>-1</sup>, the degradation efficiency only increased slightly to 91.6% and 92.1%, respectively. This indicated that using 0.25 g L<sup>-1</sup> of nZVI, the degradation efficiency was no longer significantly enhanced by superfluous fresh iron surface. Therefore, the optimum nZVI dosage of 0.25 g L<sup>-1</sup> was used in the next experiments.

### 3.2.3. Effect of H<sub>2</sub>O<sub>2</sub> concentration

The effect of H<sub>2</sub>O<sub>2</sub> concentration on the degradation of [C<sub>4</sub>mim]Br was investigated over the concentration range from 20 to 100 mmol L<sup>-1</sup> at pH 3.0 and 0.25 g L<sup>-1</sup> of nZVI dose. The results shown in Fig. 2c indicated that with the increase of H<sub>2</sub>O<sub>2</sub> concentrations from 20 to 100 mmol L<sup>-1</sup>, the degradation efficiency of [C<sub>4</sub>mim]Br first increased and then decreased, and the maximum degradation efficiency was observed at 60 mmol L<sup>-1</sup> of H<sub>2</sub>O<sub>2</sub>. This trend can be rationalized by the fact that at low concentration, H<sub>2</sub>O<sub>2</sub> could not generate enough hydroxyl radicals, and thus the degradation efficiency and degradation rate of [C<sub>4</sub>mim]Br were logically low. At the H<sub>2</sub>O<sub>2</sub> concentration of 60 mmol L<sup>-1</sup>, the degradation appeared to be most effective because more hydroxyl radicals might be formed. However, at higher concentrations of H<sub>2</sub>O<sub>2</sub>, the presence of excess H<sub>2</sub>O<sub>2</sub> induced a decrease of the degradation

efficiency due to the competition of H<sub>2</sub>O<sub>2</sub> with the IL for •OH. The reaction can be described by the equation:

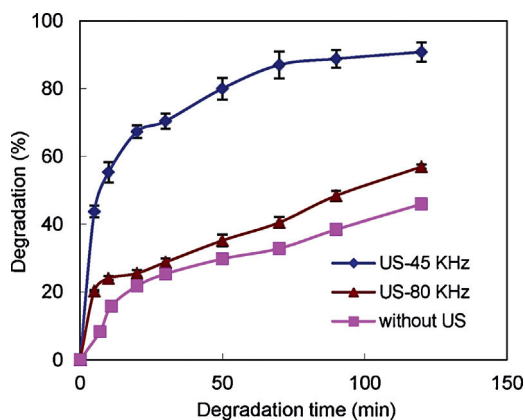


Although other radicals such as HO<sub>2</sub>• and O<sub>2</sub>•<sup>-</sup> were also generated in this system, they are much less reactive than •OH and may be neglected [24,25,29,34]. Thus, 60 mmol L<sup>-1</sup> H<sub>2</sub>O<sub>2</sub> was selected for the efficient degradation of [C<sub>4</sub>mim]Br.

In addition, we determined H<sub>2</sub>O<sub>2</sub> concentrations after 120 min degradation of [C<sub>4</sub>mim]Br by means of HPLC at different initial concentrations of H<sub>2</sub>O<sub>2</sub>. It was found that the H<sub>2</sub>O<sub>2</sub> concentrations after 120 min degradation were 14.2, 18.7, 16.9, and 20.5 mmol L<sup>-1</sup> at the initial H<sub>2</sub>O<sub>2</sub> concentrations of 20, 40, 60, and 80 mmol L<sup>-1</sup>, respectively. This indicated that during the process of IL degradation, the higher the initial H<sub>2</sub>O<sub>2</sub> concentration, the faster the H<sub>2</sub>O<sub>2</sub> decomposition, and the concentration of residual H<sub>2</sub>O<sub>2</sub> was at a similar level. In fact, the residual hydrogen peroxide after reaction can be removed by heating after being adjusted to alkalinity.

### 3.2.4. Effect of ultrasonic irradiation

The effect of ultrasonic irradiation on the degradation of [C<sub>4</sub>mim]Br was also studied under the condition: pH 3.0, 60 mmol L<sup>-1</sup> of H<sub>2</sub>O<sub>2</sub> and 0.25 g L<sup>-1</sup> of nZVI. The experiments were performed by changing the frequency of ultrasonic irradiation or without ultrasonic treatment, and the results were presented in Fig. 3. It can be seen that [C<sub>4</sub>mim]Br could be degraded in nZVI/H<sub>2</sub>O<sub>2</sub> (without US) system and the degradation efficiency was about 46% within 120 min reaction. As ultrasonic irradiation was introduced in the nZVI/H<sub>2</sub>O<sub>2</sub> system, the degradation efficiency of [C<sub>4</sub>mim]Br was enhanced, and 90.8% of [C<sub>4</sub>mim]Br was degraded at 45 kHz. It was reported that ultrasonic irradiation was able to completely destroy highly stable organic molecules by inducing chemical effects through the formation of cavitation



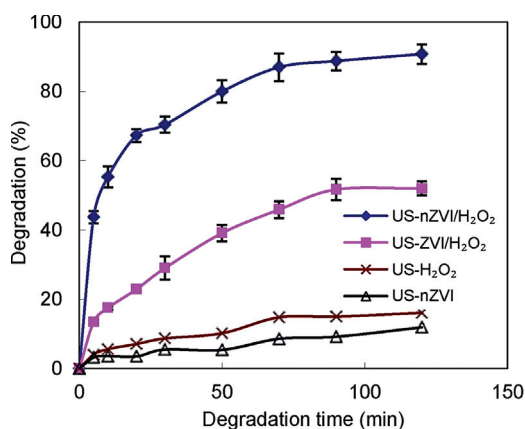
**Fig. 3.** Effect of ultrasonic frequency on the degradation of  $[C_4mim]Br$  in US-nZVI/ $H_2O_2$  system under the experimental conditions:  $[IL] = 2.0 \text{ mmol L}^{-1}$ ,  $[nZVI] = 0.25 \text{ g L}^{-1}$ ,  $[H_2O_2] = 60 \text{ mmol L}^{-1}$ , pH 3.0 and  $T = 30^\circ\text{C}$ .

microbubbles to produce a localized and transient high temperature and pressure [13,35]. The presence of ultrasonic irradiation not only improved mass transfer significantly, but also activated surface reaction in a heterogeneous system by the generated shock wave which could enhance dissolution of  $Fe^{2+}$  from iron surface and accelerate the decomposition of organic pollutants [31]. Our experimental result showed that ultrasonic treatment alone (45 kHz, without nZVI/ $H_2O_2$ ) did not have any effect on the degradation of  $[C_4mim]^+$  [36]. It can be seen from Fig. 3 that the degradation efficiency of  $[C_4mim]Br$  in US-nZVI/ $H_2O_2$  was much greater than the sum of degradation efficiency in US and nZVI/ $H_2O_2$  systems. This indicated that ultrasonic irradiation could stimulate Fenton-like reaction and a synergistic effect was obtained for the degradation of  $[C_4mim]Br$ .

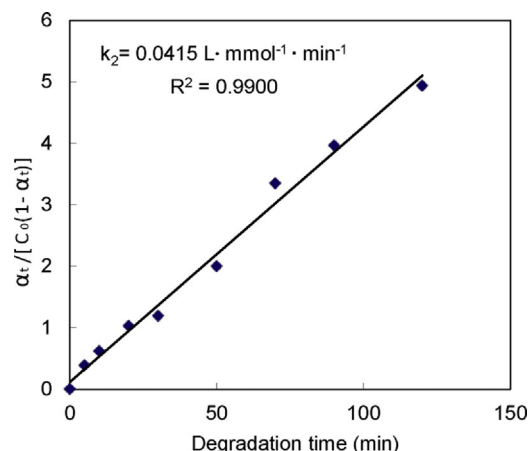
The influence of ultrasound frequency upon  $[C_4mim]Br$  degradation was examined, and the result was also shown in Fig. 3. It is noted that the degradation efficiency of  $[C_4mim]Br$  was much higher at 45 kHz than at 80 kHz, indicating that lower frequency was more conducive to the degradation of  $[C_4mim]Br$ . The possible reason is that with the increase of ultrasonic frequency, the intensity of cavitation decreased [37,38], which was less effective for the degradation of  $[C_4mim]Br$ .

### 3.2.5. Comparison of nZVI and ZVI

Finally, a comparison of nZVI with ZVI was made by using  $60 \text{ mmol L}^{-1}$  of  $H_2O_2$  and  $0.25 \text{ g L}^{-1}$  of nZVI or ZVI. At the same time, the degradation experiments of  $[C_4mim]Br$  were also



**Fig. 4.** Comparison of nZVI and ZVI on the degradation of  $[C_4mim]Br$  under the experimental conditions:  $[IL] = 2.0 \text{ mmol L}^{-1}$ ,  $[nZVI] = 0.25 \text{ g L}^{-1}$ ,  $[ZVI] = 0.25 \text{ g L}^{-1}$ ,  $[H_2O_2] = 60 \text{ mmol L}^{-1}$ , pH 3.0, ultrasound frequency = 45 kHz and  $T = 30^\circ\text{C}$ .



**Fig. 5.** The linear correlation between  $\alpha_t/[C_0(1-\alpha_t)]$  and reaction time for the second-order degradation kinetics of  $[C_4mim]Br$  in US-nZVI/ $H_2O_2$  system:  $[IL] = 2.0 \text{ mmol L}^{-1}$ ,  $[nZVI] = 0.25 \text{ g L}^{-1}$ ,  $[H_2O_2] = 60 \text{ mmol L}^{-1}$ , pH 3.0, ultrasound frequency = 45 kHz and  $T = 30^\circ\text{C}$ .

conducted only with  $0.25 \text{ g L}^{-1}$  of nZVI or  $60 \text{ mmol L}^{-1}$  of  $H_2O_2$ . All the experiments were ultrasound-assisted at 45 kHz and carried out at pH 3.0. As shown in Fig. 4,  $[C_4mim]Br$  was hardly degraded in the US-nZVI (without oxidant) and US- $H_2O_2$  (without catalyst) systems, and only 12% and 16% of degradation efficiency was obtained, respectively. Although US-ZVI/ $H_2O_2$  system was capable of degrading  $[C_4mim]Br$ , the degradation efficiency was only about 50%. Once nZVI was presented in US- $H_2O_2$  system, the degradation efficiency was remarkably increased. Thus it is appropriate to conclude that the size of iron particles played an important role in this heterogeneous Fenton-like process. The smaller the particle, the more active it was. Compared with the micro-size iron powders (325 mesh of ZVI, average diameter of  $45 \mu\text{m}$ ), nZVI showed a significantly higher catalytic activity because of its large specific surface where catalytically active sites were greatly exposed [28,39].

### 3.3. The degradation reaction kinetics of $[C_nmim]Br$

The reaction kinetic data for the degradation of  $[C_4mim]Br$  at  $30^\circ\text{C}$ , shown in Fig. 2b and c, were analyzed by the kinetic equations with different reaction orders including zero-, first-, second- and third- order. It was found that the best fitting was the second-order kinetic model. Therefore, the degradation process of  $[C_4mim]Br$  would be described by the equation:

$$\alpha_t/[C_0(1-\alpha_t)] = k_2 t \quad (5)$$

where  $\alpha_t$  is the degradation degree of  $[C_4mim]Br$  at  $t$  reaction time and can be expressed by  $\alpha_t = (C_0 - C_t)/C_0$ ,  $C_0$  is the initial concentration of the IL,  $C_t$  is the IL concentration at  $t$  reaction time, and  $k_2$  is the apparent rate constant for the degradation of  $[C_4mim]Br$ . Fig. 5 shows the linear relationship between  $\alpha_t/[C_0(1-\alpha_t)]$  and reaction time (with a correlation coefficient of 0.995) at the initial concentrations of  $0.25 \text{ g L}^{-1}$  of nZVI and  $60 \text{ mmol L}^{-1}$  of  $H_2O_2$ . It is clear that the  $k_2$  value can be determined from slope of the linear plot of  $\alpha_t/[C_0(1-\alpha_t)]$  against  $t$ . Thus obtained  $k_2$  value of  $[C_4mim]Br$  by using a linear least-square analysis was included in Table 1. The  $k_2$  values for the degradation of  $[C_4mim]Br$  at the other initial concentrations of nZVI and  $H_2O_2$  were calculated in the same way, and the results were also included in Table 1.

The data of apparent rate constants shown in Table 1 can be used to examine the effect of different initial concentrations of nZVI and  $H_2O_2$  on the degradation reaction rate of  $[C_4mim]Br$  in US-nZVI/ $H_2O_2$  system under the given reaction conditions. It can be seen from Table 1 that nZVI dosage influenced the degradation

**Table 1**  
The second order rate constants for the degradation reaction of [C<sub>n</sub>mim]Br in US-nZVI/H<sub>2</sub>O<sub>2</sub> system at 30 °C.<sup>a</sup>

IL	nZVI dose (g L <sup>-1</sup> )	H <sub>2</sub> O <sub>2</sub> concentration (mmol L <sup>-1</sup> )	k <sub>2</sub> (L mmol <sup>-1</sup> min <sup>-1</sup> )	R <sup>2</sup>
[C <sub>2</sub> mim]Br	0.25	60	0.0511	0.962
[C <sub>4</sub> mim]Br	0.25	60	0.0415	0.990
	0.50	60	0.0456	0.989
	1.0	60	0.0482	0.997
	0.25	20	0.0088	0.957
	0.25	40	0.0269	0.975
	0.25	80	0.0211	0.948
	0.25	100	0.0198	0.962
[C <sub>6</sub> mim]Br	0.25	60	0.0179	0.990
[C <sub>8</sub> mim]Br	0.25	60	0.0147	0.949
[C <sub>10</sub> mim]Br	0.25	60	0.0101	0.951

<sup>a</sup> Experimental conditions: [IL] = 2.0 mmol L, pH 3.0, ultrasonic frequency = 45 kHz.

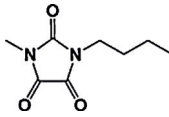
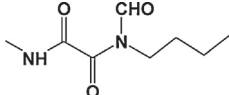
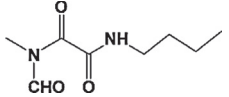
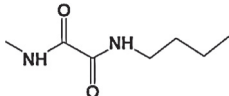
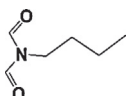
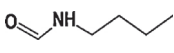
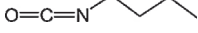
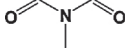
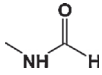
rate of [C<sub>4</sub>mim]Br to a small extent. For example, when nZVI dosage was increased from 0.25 to 1.0 g L<sup>-1</sup>, the k<sub>2</sub> values only increased from 0.0415 to 0.0482 L mmol<sup>-1</sup> min<sup>-1</sup> at the initial H<sub>2</sub>O<sub>2</sub> concentration of 60 mmol L<sup>-1</sup>. However, the initial concentration of H<sub>2</sub>O<sub>2</sub> was found to have a significant influence. At a given nZVI dosage of 0.25 g L<sup>-1</sup>, the apparent rate constants increased from 0.0088 to 0.0415, and then decreased to 0.0198 L mmol<sup>-1</sup> min<sup>-1</sup> with the increase of the initial H<sub>2</sub>O<sub>2</sub> concentrations from 20 to 100 mmol L<sup>-1</sup>, and a maximum value was observed at 60 mmol L<sup>-1</sup>. These trends were in agreement with those of the initial concentration effects of nZVI and H<sub>2</sub>O<sub>2</sub> in the degradation efficiency of [C<sub>4</sub>mim]Br discussed before.

[C<sub>n</sub>mim]Br (n = 2, 6, 8, and 10) were also degraded to study the degradation reaction kinetics of the imidazolium ILs under the above optimal experimental conditions, and the results were

shown in Fig. 6. It can be seen that >93% of [C<sub>2</sub>mim]Br was degraded during 120 min and the degradation degree of [C<sub>4</sub>mim]Br was slightly lower. However, [C<sub>10</sub>mim]Br was more resistant to the oxidation by •OH, and only 73.7% of the IL was removed within 120 min reaction. These results suggest that oxidation degree of the imidazolium ILs was structure-dependent, and was dependent on the alkyl chain length substituted at the N-1-position. Degradability of the ILs in this system decreased in the order: [C<sub>2</sub>mim]Br > [C<sub>4</sub>mim]Br > [C<sub>6</sub>mim]Br > [C<sub>8</sub>mim]Br > [C<sub>10</sub>mim]Br, which is consistent with the results reported by Stepnowski and co-workers [12,16].

Similarly, the data of degradation degree (α<sub>t</sub>) of [C<sub>n</sub>mim]Br (n = 2, 6, 8, and 10) and responding degradation reaction time were also fitted by the degradation reaction kinetics equations with different reaction orders. The results showed that like

**Table 2**  
The degradation intermediates of [C<sub>4</sub>mim]Br in US-nZVI/H<sub>2</sub>O<sub>2</sub> system detected by GC-MS.

Intermediate	Retention time (min)	Characteristic fragment(m/z)	Molecular structure	Molecular weight
<b>a</b>	13.77	56,129,184		184
<b>b</b>	13.36	58,30,186		186
<b>c</b>	14.11	128,57,30		186
<b>d</b>	12.66	58, 100,158		158
<b>f</b>	8.13	58,30,129		129
<b>g</b>	7.73	58,30,101		101
<b>h</b>	8.78	41,99		99
<b>i</b>	4.48	59,30		87
<b>j</b>	3.96	59,30		59

**Table 3**The degradation intermediates of [C<sub>n</sub>mim]Br (n = 2, 6, 8, and 10) in US-nZVI/H<sub>2</sub>O<sub>2</sub> system obtained from GC–MS analyses at 20, 40, 70, and 120 min of reaction time.

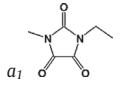
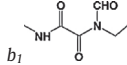
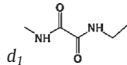
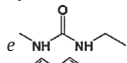
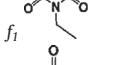
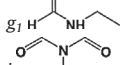
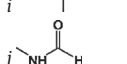
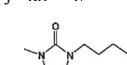
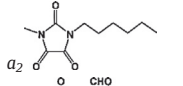
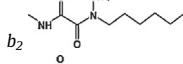
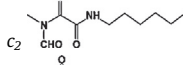
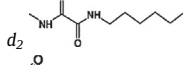
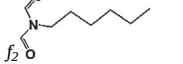
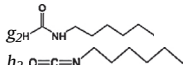
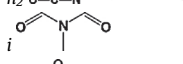
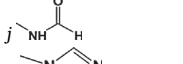
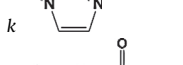
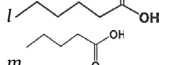
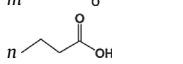
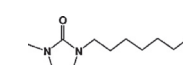
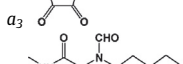
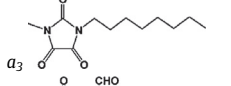
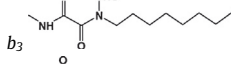
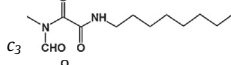
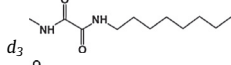
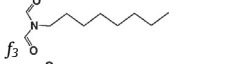
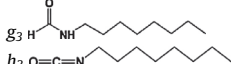
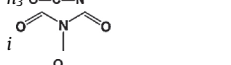


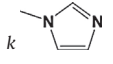
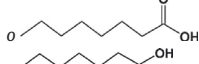
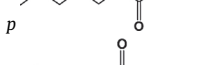
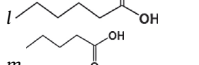
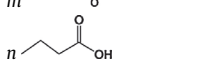
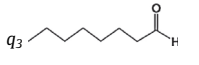
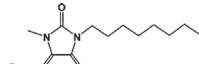
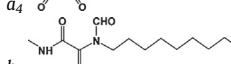
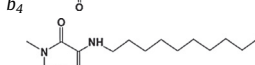
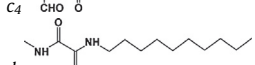
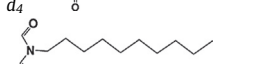
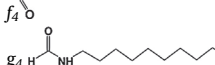
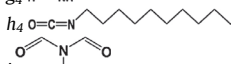

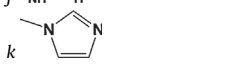


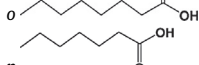
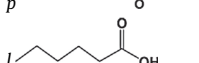
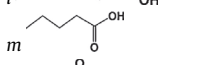
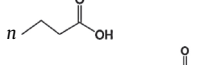
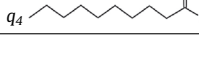
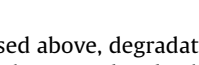
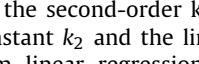
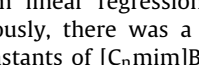
IL	Intermediate	Retention time (min)	Main fragment (m/z)	Peak area of main fragment ( $\times 10^5$ )				
				20 min	40 min	70 min	120 min	
[C <sub>2</sub> mim]Br		11.39 ± 0.04	56	37.37	88.40	119.3	166.0	
		11.06 ± 0.03	58	138.0	199.9	176.1	156.9	
		9.95 ± 0.03	58	0.34	0.48	0.34	0.22	
		8.47 ± 0.03	58	0.65	1.26	1.60	2.44	
		5.22 ± 0.02	73	40.54	57.56	56.52	62.39	
		4.70 ± 0.02	73	4.18	6.25	5.34	10.15	
		4.53 ± 0.02	59	16.04	22.17	23.05	22.78	
		3.98 ± 0.02	59	2.59	3.67	4.94	5.63	
	[C <sub>6</sub> mim]Br		16.14 ± 0.04	56	7.15	5.78	2.36	ND <sup>a</sup>
			15.76 ± 0.05	58	24.11	17.97	5.35	ND <sup>a</sup>
		16.51 ± 0.05	128	3.74	2.85	0.73	ND <sup>a</sup>	
		15.22 ± 0.04	128	15.64	12.25	3.72	0.35	
		11.12 ± 0.03	58	17.97	11.11	3.31	0.23	
		10.84 ± 0.04	58	33.71	18.54	5.04	0.46	
		11.75 ± 0.04	99	3.58	7.35	8.95	3.94	
		4.54 ± 0.02	59	8.90	10.96	14.37	15.86	
		3.98 ± 0.02	59	8.26	13.30	15.79	12.57	
		6.13 ± 0.03	82	4.39	3.02	0.98	0.11	
		7.37 ± 0.03	60	4.10	3.72	1.71	0.37	
		5.91 ± 0.02	60	0.38	0.68	0.77	0.60	
		4.56 ± 0.02	60	1.05	2.12	5.77	8.22	
[C <sub>8</sub> mim]Br			18.40 ± 0.06	142	7.70	5.51	1.44	0.14
		18.02 ± 0.05	60	16.90	15.31	2.94	0.35	
		18.77 ± 0.05	156	8.93	5.40	0.58	0.09	
		17.55 ± 0.06	156	20.41	14.18	1.04	0.26	
		13.88 ± 0.04	74	21.57	13.32	1.63	0.10	
		13.65 ± 0.04	58	61.58	34.98	5.04	0.75	
		14.37 ± 0.05	99	7.83	15.71	14.55	2.53	
		4.52 ± 0.02	59	9.18	11.96	14.49	16.59	
		3.97 ± 0.02	59	8.76	18.35	20.16	17.11	

Table 3 (Continued)

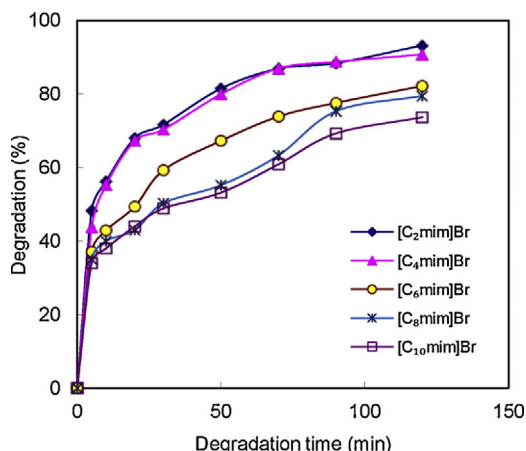
IL	Intermediate	Retention time (min)	Main fragment (m/z)	Peak area of main fragment ( $\times 10^5$ )			
				20 min	40 min	70 min	120 min
[C <sub>10</sub> mim]Br		6.01 ± 0.03	82	13.24	15.47	5.40	1.55
		10.27 ± 0.04	60	1.16	1.81	0.42	ND <sup>a</sup>
		8.89 ± 0.04	60	0.32	0.86	0.31	ND <sup>a</sup>
		7.44 ± 0.04	60	0.47	1.26	0.97	0.48
		5.87 ± 0.03	60	0.39	2.72	3.76	2.06
		4.47 ± 0.03	60	2.84	9.48	17.04	19.60
		6.83 ± 0.03	43	0.91	0.73	ND <sup>a</sup>	ND <sup>a</sup>
		20.45 ± 0.08	142	17.12	6.64	3.12	0.41
		20.10 ± 0.08	60	22.88	14.53	7.47	0.84
		20.79 ± 0.07	184	2.96	1.88	0.84	0.39
		19.66 ± 0.06	184	35.64	23.32	10.48	1.24
		16.35 ± 0.04	74	22.91	12.39	5.33	0.71
		16.16 ± 0.05	59	17.32	9.34	3.73	0.47
		16.89 ± 0.04	99	34.52	31.28	18.54	4.59
		4.51 ± 0.02	59	15.25	18.84	20.38	20.86
		3.96 ± 0.02	59	28.23	35.20	36.32	33.45
		6.11 ± 0.03	82	82.22	76.93	38.52	11.84
		12.89 ± 0.07	60	2.59	1.21	0.46	0.14
		11.58 ± 0.06	60	0.98	0.88	0.43	0.28
		10.24 ± 0.08	60	0.88	0.98	0.61	0.49
		8.81 ± 0.06	60	1.48	2.01	1.61	0.97
		7.35 ± 0.03	60	3.16	5.36	5.50	4.24
		5.87 ± 0.02	60	3.29	7.49	8.87	11.09
	4.48 ± 0.02	60	7.04	12.08	17.43	31.40	
	9.96 ± 0.03	43	2.11	1.51	1.04	0.45	

<sup>a</sup> ND: not detected.

[C<sub>4</sub>mim]Br discussed above, degradation of [C<sub>n</sub>mim]Br ( $n=2, 6, 8,$  and 10) followed the second-order kinetic model. The values of apparent rate constant  $k_2$  and the linear correlation coefficients ( $R$ ) obtained from linear regression analysis were also listed in Table 1. Obviously, there was a significant decrease in the apparent rate constants of [C<sub>n</sub>mim]Br with the increase of alkyl chain length. This indicated that lengthening the substituent of an imidazolium ionic liquid at position N-1 increased the resistance to chemical degradation. In the cations of the ILs, both the side chain and the imidazolium core would be targeted by •OH

radical attack. When the substituted side chain was longer, the imidazolium core was less likely to be attacked by •OH radicals [40]. Similar results have been reported for the degradation of imidazolium ILs in UV, UV/H<sub>2</sub>O<sub>2</sub> and Fenton-like systems [12,16]. However, these results are not consistent with our previous report [32], in which no strong alkyl chain length dependence of the apparent rate constants of the ILs was observed in the US-ZVI/AC system, although they decreased slightly in the order: [C<sub>6</sub>mim]Br > [C<sub>10</sub>mim]Br ≈ [C<sub>8</sub>mim]Br > [C<sub>4</sub>mim]Br ≈ [C<sub>2</sub>mim]Br. The possible reason is that in the US-ZVI/AC system, synergic





**Fig. 6.** Effect of alkyl chain length on the degradation of  $[C_n\text{mim}]\text{Br}$  ( $n=2,4,6,8,10$ ) in US-nZVI/ $\text{H}_2\text{O}_2$  system under the experimental conditions:  $[\text{IL}]=2.0\text{ mmol L}^{-1}$ ,  $[\text{nZVI}]=0.25\text{ g L}^{-1}$ ,  $[\text{H}_2\text{O}_2]=60\text{ mmol L}^{-1}$ , pH 3.0, ultrasound frequency = 45 kHz and  $T=30^\circ\text{C}$ .

effect of ultrasonic cavitations and ZVI/AC galvanic cells on the degradation of the imidazolium ILs reduced the hydrophobic effect of the ILs. Therefore, the degradation degree and degradation rate of  $[C_n\text{mim}]\text{Br}$  in the US-ZVI/AC system were less influenced by their alkyl chain length.

Additionally, a comparison has been made for the apparent rate constant of  $[C_n\text{mim}]\text{Br}$  in US-nZVI/ $\text{H}_2\text{O}_2$  and US-ZVI/AC systems. It was found that the degradation reaction rate of  $[C_2\text{mim}]\text{Br}$  and  $[C_4\text{mim}]\text{Br}$  was faster in US-nZVI/ $\text{H}_2\text{O}_2$  system than in US-ZVI/AC system, while that of  $[C_6\text{mim}]\text{Br}$ ,  $[C_8\text{mim}]\text{Br}$ , and  $[C_{10}\text{mim}]\text{Br}$  was much slower in US-nZVI/ $\text{H}_2\text{O}_2$  system. This observation confirmed again that degradation reaction rate of the imidazolium ILs were more dependent on the alkyl chain length in the Fenton-like system than in the ZVI/AC system.

### 3.4. Analysis of degradation intermediates and pathway for $[C_4\text{mim}]\text{Br}$

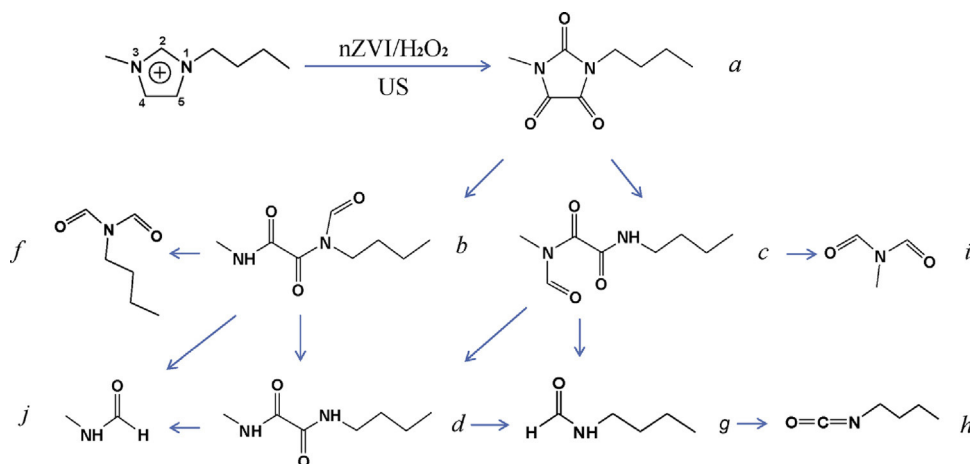
Analysis of intermediates by GC-MS was carried out at 20, 40, 70, and 120 min degradation of  $[C_4\text{mim}]\text{Br}$  in the US-nZVI/ $\text{H}_2\text{O}_2$  system. The structures of nine intermediates identified by GC-MS were shown in Table 2 and their mass spectra were provided in Figs. S1–S9 (available in Appendix A. Supplementary data). It is predicted that intermediate 1-butyl-3-methyl-2,4,5-trioxoimidazolidine (**a**) was a product resulted from the oxidation of the imidazolium ring,

and the oxidized ring opened to give product **b** and **c**. The intermediate **d** was a diamide, obtained by eliminating the formaldehyde group of **b** and **c**, and could be further degraded to give **f**, **j**, and **g**. The intermediate **h** was from the dehydrogenation of **g**, and **a** could also be decomposed into **i** and **g**. It is well known that the peak area of main fragment of the intermediate can be used to estimate its concentration. The results of the peak area (data not displayed) showed that most intermediates were abundant at the degradation time of 20 min, but their concentrations decreased with further increase of reaction time and vanished at 120 min degradation. However, concentrations of the intermediates **i** and **j** peaked at 40 min degradation and then they gradually attenuated.

According to the structure and concentration trends of the degradation products, a postulated degradation pathway was presented for  $[C_4\text{mim}]^+$  cation in Fig. 7. It is clear that the imidazolium ring was first oxidized in positions C2, C4, and C5 into three carbonyl groups to form product **a**, and this has been supported by the previous reports [13,36,41,42]. It can be expected that product **a** was not stable against further oxidation and would tend to degrade subsequently. The favorable oxidative cleavage of the C–N bond happened at C2–N3 or C2–N1 in the ring and induced the opening of the heterocyclic ring to give products **b** and **c**. Although X-ray data showed that the bond lengths of N1–C2 and C2–N3 are significantly shorter than those of N1–C5 and N3–C4 in the ring of  $[C_4\text{mim}]^+$  cation [43,44], oxidative cleavages of N1–C5 and N3–C4 bonds on the ring of intermediate **a** were not observed, and this is possible because product **a** may have a cyclic conjugated system, where lower electron density in N1–C2 and C2–N3 made them easy to be attacked. The formaldehyde groups of **b** and **c** then broke away and **d** was generated. The cleavage between two amide bonds in compounds **b**, **c**, and **d** led to the formation of products **f** and **j**, **g** and **i**, and **j** and **g**, respectively. Then the intermediate **g** might be dehydrogenated under the action of OH radicals to give **h**. Coincidentally, Gao et al. [42] found that **a**, **g**, and **i** were the intermediates of  $[C_4\text{mim}]\text{Cl}$  in plasma electrolysis system and six products were detected in their work.

### 3.5. Degradation intermediates and pathways for the other imidazolium ILs

Intermediate products produced in the degradation processes of  $[C_n\text{mim}]\text{Br}$  ( $n=2, 6, 8, \text{ and } 10$ ) were also analyzed using GC-MS at 20, 40, 70, and 120 min of the degradation. The chemical structures of intermediates identified were shown in Table 3. It was shown that more degradation products were detected by GC-MS for the ILs with longer side chain, and the number of interme-



**Fig. 7.** The degradation pathway suggested for  $[C_4\text{mim}]^+$  in US-nZVI/ $\text{H}_2\text{O}_2$  system.

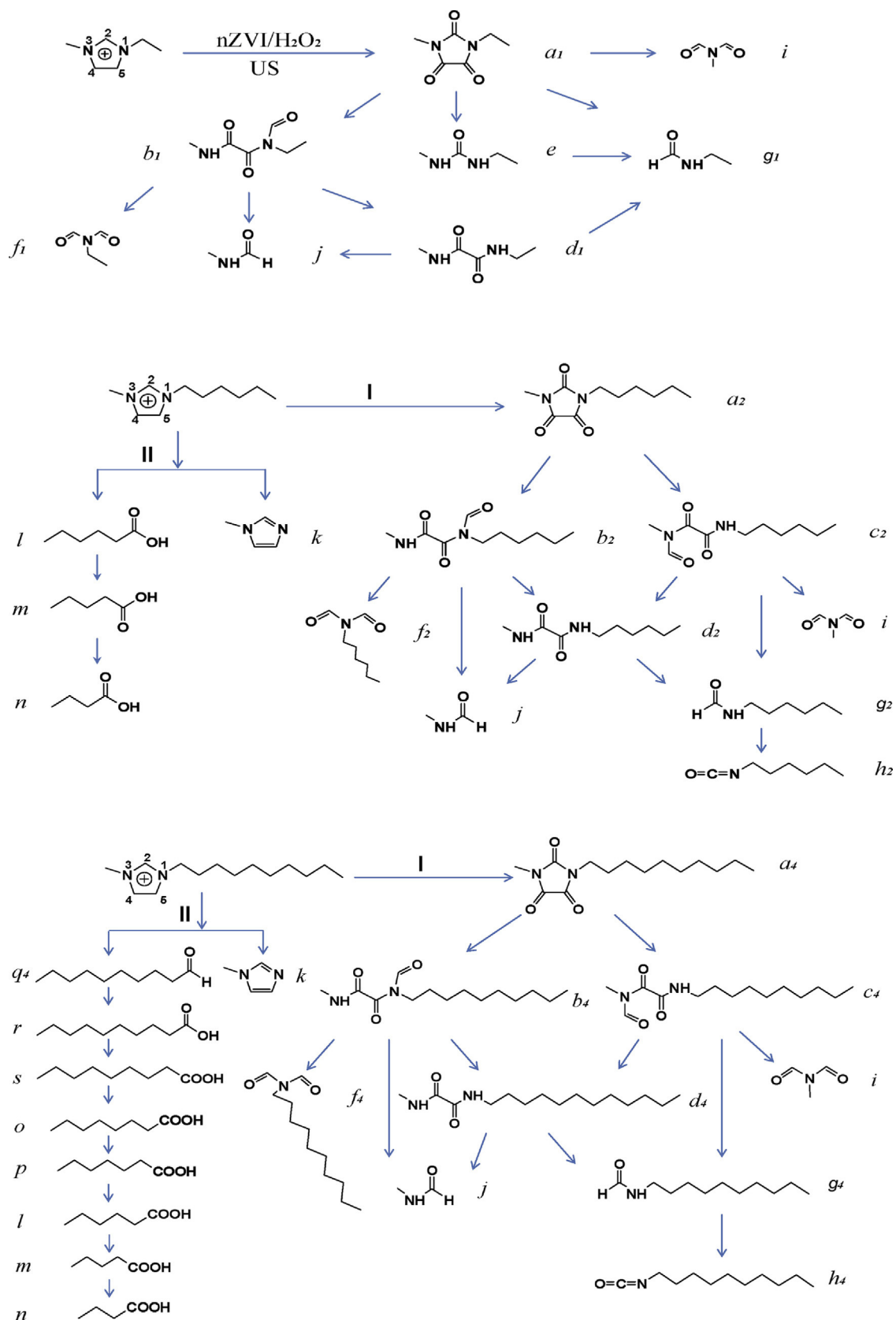


Fig. 8. The degradation pathway suggested for  $[C_2mim]^+$ ,  $[C_6mim]^+$ , and  $[C_{10}mim]^+$  in US-nZVI/H<sub>2</sub>O<sub>2</sub> system.

diates was 8, 13, 16, and 18 for the degradation of [C<sub>2</sub>mim]Br, [C<sub>6</sub>mim]Br, [C<sub>8</sub>mim]Br, and [C<sub>10</sub>mim]Br, respectively. The data of peak area of their main fragments at different reaction time were also listed in Table 3. Compared with the degradation of [C<sub>4</sub>mim]Br, the same intermediates *N*-formyl-*N*-methylformamide (**i**) and *N*-methylformamide (**j**) were detected, and some similar intermediates such as **a**, **b**, **c**, **d**, **f**, **g**, and **h** were also identified. It can be seen that the concentrations for most of the degradation products increased in the initial stage of the reaction and then decreased, and the downward trend illustrated further decomposition of the intermediates. It was also observed that the concentrations of **i** and **n** continuously went up with the increase of the reaction time and meanwhile, the concentration of **j** produced from the degradation of [C<sub>6</sub>mim]Br, [C<sub>8</sub>mim]Br, and [C<sub>10</sub>mim]Br peaked at 70 min degradation and then slowly diminished. This clearly suggested that **i**, **j**, and **n** were likely to be the late-stage products from oxidation of the imidazolium ILs.

As a result, similar pathways were suggested for the degradation of [C<sub>2</sub>mim]Br, [C<sub>6</sub>mim]Br, and [C<sub>10</sub>mim]Br (Fig. 8). It is predictable that the degradation pathway of [C<sub>8</sub>mim]<sup>+</sup> was similar to that of [C<sub>10</sub>mim]<sup>+</sup> because of their complete identical degradation products. Notably, compound 1-ethyl-3-methyl-urea (**e**) had been detected in the degradation process of [C<sub>2</sub>mim]Br, but no similar product was found for [C<sub>4</sub>mim]Br, [C<sub>6</sub>mim]Br, [C<sub>8</sub>mim]Br, and [C<sub>10</sub>mim]Br. This demonstrated that in the degradation process of [C<sub>2</sub>mim]Br, **e** could be formed by simultaneously breaking of N1–C5 and N3–C4 in the oxidized ring of **a**<sub>1</sub>, in which each of the five bonds on the ring might be broken to generate subsequent four degradation products **b**<sub>1</sub>, **e**, **g**<sub>1</sub>, and **i**. However, in the degradation process of [C<sub>*n*</sub>mim]Br (*n* = 4, 6, 8, and 10), further oxidation of the first product **a** took place only through the cleavage of N1–C2 and C2–N3 bonds on the oxidized imidazolium ring. At this stage, it can be speculated that the ethyl is more similar to methyl in [C<sub>2</sub>mim]Br, and each of the five bonds on the ring of **a**<sub>1</sub> has the chance to be attacked.

Unlike the degradation of [C<sub>4</sub>mim]Br, another degradation pathway for [C<sub>6</sub>mim]Br, [C<sub>8</sub>mim]Br and [C<sub>10</sub>mim]Br was suggested according to the identified intermediates: the cleavage of *N*-alkyl side chain and the formation of *N*-methylimidazole (**k**). The alkyl side chain was successively oxidized to the corresponding aldehyde and carboxylic acid, and the latter was likely to be decarboxylated to form shorter-chain carboxylic acid step by step, and the final carboxylic acid detected by GC–MS is butyric acid. It was noted that concentrations of the detected *N*-methylimidazole (**k**) and butyric acid (**n**) increased with lengthening alkyl side chain. This illustrated that the longer the alkyl side chain, the easier the breakage of the N–C bond in the *N*-alkyl side chain.

It is therefore believed that the degradation pathway of [C<sub>*n*</sub>mim]Br was structure-related. For [C<sub>2</sub>mim]Br and [C<sub>4</sub>mim]Br, the main degradation pathway was oxidation of the imidazolium ring and subsequent ring-opening. But for [C<sub>6</sub>mim]Br, [C<sub>8</sub>mim]Br, and [C<sub>10</sub>mim]Br, a more complex degradation process was revealed, and the degradation through the breakage of the N–C bond in the *N*-alkyl side chain became important. This is different from the previous reports on the degradation of 1-alkyl-3-methylimidazolium ILs in US–H<sub>2</sub>O<sub>2</sub>/CH<sub>3</sub>COOH [13], US–ZVI/AC [32] and plasma electrolysis systems [42]. For example, in our previous work, three intermediates and the same degradation pathway were observed for the degradation of each of [C<sub>*n*</sub>mim]Br (*n* = 2, 4, 6, 8, and 10) in US–ZVI/AC system [32]. Although ultrasonic irradiation and zero-valent iron were both employed in US–nZVI/H<sub>2</sub>O<sub>2</sub> and US–ZVI/AC systems, US–ZVI/AC systems is a combination of ultrasonic irradiation and ZVI/AC internal micro-electrolysis, whereas US–nZVI/H<sub>2</sub>O<sub>2</sub> is a combination of ultrasonic irradiation and Fenton-like process. The difference in the degradation efficiency, degradation rate and degradation intermediates of the ILs

in the two different systems may be resulted from their difference in the nature of chemical reactions. In the current literatures, few investigations have been reported to study the degradation intermediates of imidazolium ILs. Limited results also showed that the use of different degradation methods might result in different degradation products and pathways [40,45–47].

As mentioned above, the degradation rate of [C<sub>*n*</sub>mim]Br in the US–nZVI/H<sub>2</sub>O<sub>2</sub> system was in the order [C<sub>2</sub>mim]Br > [C<sub>4</sub>mim]Br > [C<sub>6</sub>mim]Br > [C<sub>8</sub>mim]Br > [C<sub>10</sub>mim]Br. However, the order for the degradation rate of their intermediate products was not synchronous with the degradation rate of [C<sub>*n*</sub>mim]Br themselves: decomposition rate of the intermediates of [C<sub>4</sub>mim]Br was very fast, that of [C<sub>6</sub>mim]Br was slightly slower, and that of [C<sub>2</sub>mim]Br was the slowest. This demonstrated that [C<sub>2</sub>mim]Br could quickly be oxidized, but its intermediate products were relatively stable. In addition, it should be stressed that the final degradation products **i**, **j**, **n**, and **k** are commonly low-toxic organic species and can be used in the pharmaceutical and chemical industry. Dominguez et al. [14] also reported that Fenton oxidation allowed the almost complete abatement of the ecotoxicity even in the cases of the highly ecotoxic ILs with long alkyl chain.

#### 4. Conclusions

Our results indicate that the degradation of [C<sub>*n*</sub>mim]Br (*n* = 2, 4, 6, 8, and 10) in the ultrasound-assisted nZVI/H<sub>2</sub>O<sub>2</sub> system is dependent on the length of the alkyl side chain, and can be described by the second order kinetic model. In the degradation process, 8, 9, 13, 16, and 18 intermediates were detected by GC–MS for [C<sub>2</sub>mim]Br, [C<sub>4</sub>mim]Br, [C<sub>6</sub>mim]Br, [C<sub>8</sub>mim]Br, and [C<sub>10</sub>mim]Br, respectively. Based on these intermediate products, detailed pathways were proposed for the degradation of [C<sub>*n*</sub>mim]Br. To the best of our knowledge, the present study is the first report to illustrate the degradation pathways and kinetics of imidazolium ILs in US–nZVI/H<sub>2</sub>O<sub>2</sub> system. It is believed that these results could be useful for developing Fenton-like process handling of ILs in aqueous solutions.

#### Acknowledgements

This work is supported from the National Natural Science Foundation of China (No. 210273062 and 21133009) and the Doctoral Foundation of Henan University of Science and Technology.

#### Appendix A. Supplementary data

Supplementary data associated with this article can be found, in the online version, at <http://dx.doi.org/10.1016/j.jhazmat.2014.10.050>.

#### References

- [1] H. Olivier-Bourbigou, L. Magna, Ionic liquids: perspectives for organic and catalytic reactions, *J. Mol. Catal. A* 182 (2002) 419–437.
- [2] A.B. McEwen, H.L. Ngo, K. LeCompte, J.L. Goldman, Electrochemical properties of imidazolium salt electrolytes for electrochemical capacitor applications, *J. Electrochem. Soc.* 146 (1999) 1687–1695.
- [3] H. Huang, H. Wang, G. Wei, I. Sun, J. Huang, Y. Yang, Extraction of nanosize copper pollutants with an ionic liquid, *Environ. Sci. Technol.* 40 (2006) 4761–4764.
- [4] T.P.T. Pham, C.-W. Cho, Y.-S. Yun, Environmental fate and toxicity of ionic liquids: a review, *Water Res.* 44 (2010) 352–372.
- [5] G. Quijano, A. Couvert, A. Amrane, G. Darracq, C. Couriol, P.L. Cloirec, L. Paquin, D. Carrie, Toxicity and biodegradability of ionic liquids: new perspectives towards whole-cell biotechnological applications, *Chem. Eng. J.* 174 (2011) 27–32.
- [6] A. Romero, A. Santos, J. Tojo, A. Rodríguez, Toxicity and biodegradability of imidazolium ionic liquids, *J. Hazard. Mater.* 151 (2008) 268–273.

- [7] D. Coleman, N. Gathergood, Biodegradation studies of ionic liquids, *Chem. Soc. Rev.* 39 (2011) 600–637.
- [8] T.P.T. Pham, C.-W. Cho, C.-O. Jeon, Y.-J. Chung, M.-W. Lee, Y.-S. Yun, Identification of metabolites involved in the biodegradation of the ionic liquid 1-butyl-3-methylpyridinium bromide by activated sludge microorganisms, *Environ. Sci. Technol.* 43 (2009) 516–521.
- [9] N. Gathergood, M.T. Garcia, P.J. Scammells, Biodegradable ionic liquids. Part I. Concept, preliminary targets and evaluation, *Green Chem.* 6 (2004) 166–175.
- [10] N. Gathergood, P.J. Scammells, M.T. Garcia, Biodegradable ionic liquids. Part III. The first readily biodegradable ionic liquids, *Green Chem.* 8 (2006) 156–160.
- [11] S. Stolte, S. Abdulkarim, J. Arning, A.-K. Blomeyer-Nienstedt, U. Bottin-Weber, M. Matzke, J. Ranke, B. Jastorff, J. Thöming, Primary biodegradation of ionic liquids cations, identification of degradation products of 1-methyl-3-octylimidazolium chloride and electrochemical wastewater treatment of poorly biodegradable compounds, *Green Chem.* 10 (2008) 214–224.
- [12] P. Stepnowski, A. Zaleska, Comparison of different advanced oxidation processes for the degradation of room temperature ionic liquids, *J. Photochem. Photobiol. A* 170 (2005) 45–50.
- [13] X. Li, J. Zhao, Q. Li, L. Wang, S. Tsang, Ultrasonic chemical oxidative degradation of 1,3-dialkylimidazolium ionic liquids and their mechanistic elucidation, *Dalton Trans.* 36 (2007) 1875–1880.
- [14] C.M. Dominguez, M. Munoz, A. Quintanilla, Z.M. Pedro, S.P.M. Ventura, J.A.P. Coutinho, J.A. Casas, J.J. Rodriguez, Degradation of imidazolium-based ionic liquids in aqueous solution by Fenton oxidation, *J. Chem. Technol. Biotechnol.* (2014), <http://dx.doi.org/10.1002/jctb.4366>.
- [15] E.M. Siedlecka, W. Mroziak, Z. Kaczynski, P. Stepnowski, Degradation of 1-butyl-3-methylimidazolium chloride ionic liquid in a Fenton-like system, *J. Hazard. Mater.* 154 (2008) 893–900.
- [16] E.M. Siedlecka, P. Stepnowski, The effect of alkyl chain length on the degradation of alkylimidazolium- and pyridinium-type ionic liquids in a Fenton-like system, *Environ. Sci. Pollut. Res.* 16 (2009) 453–458.
- [17] E.M. Siedlecka, M. Gołębowski, Z. Kaczynski, J. Czupryniak, T. Ossowski, P. Stepnowski, Degradation of ionic liquids by Fenton reaction; the effect of anions as counter and background ions, *Appl. Catal. B Environ.* 91 (2009) 573–579.
- [18] S. Esplugas, J. Giménez, S. Contreras, E. Pascual, M. Rodríguez, Comparison of different advanced oxidation processes for phenol degradation, *Water Res.* 36 (2002) 1034–1042.
- [19] J.A. Zazo, J.A. Casas, A.F. Mohedano, M.A. Gilarranz, J.J. Rodriguez, Chemical pathway and kinetics of phenol oxidation by Fenton's reagent, *Environ. Sci. Technol.* 39 (2005) 9295–9302.
- [20] G. Plięgo, J.A. Zazo, J.A. Casas, J.J. Rodriguez, Treatment of highly polluted hazardous industrial wastewaters by combined coagulation-adsorption and high-temperature Fenton oxidation, *Ind. Eng. Chem. Res.* 51 (2012) 2888–2896.
- [21] E.M. Siedlecka, M. Gołębowski, J. Kumirska, P. Stepnowski, Identification of 1-butyl-3-methylimidazolium chloride degradation products formed in Fe(III)/H<sub>2</sub>O<sub>2</sub> oxidation system, *Chem. Anal. (Warsaw)* 53 (2008) 943–951.
- [22] H.S. Son, J.K. Im, K.D. Zoh, A Fenton-like degradation mechanism for 1,4-dioxane using zero-valent iron (Fe<sup>0</sup>) and UV light, *Water Res.* 43 (2009) 1457–1463.
- [23] M. Kallel, C. Belaid, T. Mechichi, M. Ksibi, B. Elleuch, Removal of organic load and phenolic compounds from olive mill wastewater by Fenton oxidation with zero-valent iron, *Chem. Eng. J.* 150 (2009) 391–395.
- [24] N.K. Daud, B.H. Hameed, Decolorization of Acid Red 1 by Fenton-like process using rice husk ash-based catalyst, *J. Hazard. Mater.* 176 (2010) 938–944.
- [25] T. Zhou, Y.Z. Li, J. Ji, F.-S. Wong, X.H. Lu, Oxidation of 4-chlorophenol in a heterogeneous zero valent iron/H<sub>2</sub>O<sub>2</sub> Fenton-like system: kinetic, pathway and effect factors, *Sep. Purif. Technol.* 62 (2008) 551–558.
- [26] F.C.C. Moura, M.H. Araujo, R.C.C. Costa, J.D. Fabris, J.D. Ardisson, W.A.A. Macedo, R.M. Lago, Efficient use of Fe metal as an electron transfer agent in a heterogeneous Fenton system based on Fe<sup>0</sup>/Fe<sub>3</sub>O<sub>4</sub> composites, *Chemosphere* 60 (2005) 1118–1123.
- [27] E.G. Garrido-Ramírez, B.K.G. Theng, M.L. Mora, Clays and oxide minerals as catalysts and nanocatalysts in Fenton-like reactions—a review, *Appl. Clay Sci.* 47 (2010) 182–192.
- [28] J.T. Nurmi, P.G. Tratnyek, V. Sarathy, D.R. Baer, J.E. Amonette, K. Pecher, C. Wang, J.C. Linehan, D.W. Matson, R.L. Penn, M.D. Driessen, Characterization and properties of metallic iron nanoparticles: spectroscopy, electrochemistry, and kinetics, *Environ. Sci. Technol.* 39 (2005) 1221–1230.
- [29] L. Xu, J. Wang, A heterogeneous Fenton-like system with nanoparticulate zero-valent iron for removal 4-chloro-3-methyl phenol, *J. Hazard. Mater.* 186 (2011) 256–264.
- [30] J. Liang, S. Komarov, N. Hayashi, E. Kasai, Improvement in sonochemical degradation of 4-chlorophenol by combined use of Fenton-like reagents, *Ultrason. Sonochem.* 14 (2007) 201–207.
- [31] T. Zhou, Y.Z. Li, F.-S. Wong, X.H. Lu, Enhanced degradation of 2,4-dichlorophenol by ultrasound in a new Fenton like system (Fe/EDTA) at ambient circumstance, *Ultrason. Sonochem.* 15 (2008) 782–790.
- [32] H.M. Zhou, P. Lv, Y.Y. Shen, J.J. Wang, J. Fan, Identification of degradation products of ionic liquids in an ultrasound assisted zero-valent iron activated carbon micro-electrolysis system and their degradation mechanism, *Water Res.* 47 (2013) 3514–3522.
- [33] Y.H. Huang, T.C. Zhang, Effects of dissolved oxygen on formation of corrosion products and concomitant oxygen and nitrate reduction in zero-valent iron systems with or without aqueous Fe<sup>2+</sup>, *Water Res.* 39 (2005) 1751–1760.
- [34] N. Masomboon, C. Ratanatamskul, M.C. Lu, Chemical oxidation of 2,6-dimethylaniline in the Fenton process, *Environ. Sci. Technol.* 43 (2009) 8629–8634.
- [35] P. Ning, H.-J. Bart, Y.J. Jiang, A. de Haan, C. Tien, Treatment of organic pollutants in coke plant wastewater by the method of ultrasonic irradiation, catalytic oxidation and activated sludge, *Sep. Purif. Technol.* 41 (2005) 133–139.
- [36] H.M. Zhou, Y.Y. Shen, P. Lv, J.J. Wang, J. Fan, Degradation of 1-butyl-3-methylimidazolium chloride ionic liquid by ultrasound and zero-valent iron/activated carbon, *Sep. Purif. Technol.* 104 (2013) 208–213.
- [37] G.O.H. Whillock, B.F. Harvey, Ultrasonically enhanced corrosion of 304L stainless steel II: the effect of frequency, acoustic power and horn to specimen distance, *Ultrason. Sonochem.* 4 (1997) 33–38.
- [38] M.-L. Doche, J.-Y. Hihn, A. Mandroyan, R. Viennet, F. Touyeras, Influence of ultrasound power and frequency upon corrosion kinetics of zinc in saline media, *Ultrason. Sonochem.* 10 (2003) 357–362.
- [39] R. Cheng, J.L. Wang, W.X. Zhang, Comparison of reductive dechlorination of *p*-chlorophenol using Fe<sup>0</sup> and nanosized Fe<sup>0</sup>, *J. Hazard. Mater.* 144 (2007) 334–339.
- [40] E.M. Siedlecka, S. Stolte, M. Gołębowski, A. Nienstedt, P. Stepnowski, J. Thöming, Advanced oxidation process for the removal of ionic liquids from water: the influence of functionalized side chains on the electrochemical degradability of imidazolium cations, *Sep. Purif. Technol.* 101 (2012) 26–33.
- [41] A. Fabiańska, T. Ossowski, P. Stepnowski, S. Stolte, J. Thöming, E.M. Siedlecka, Electrochemical oxidation of imidazolium-based ionic liquids: the influence of anions, *Chem. Eng. J.* 198–199 (2012) 338–345.
- [42] J. Gao, L. Chen, Y. He, Z. Yan, X. Zheng, Degradation of imidazolium-based ionic liquids in aqueous solution using plasma electrolysis, *J. Hazard. Mater.* 265 (2014) 261–270.
- [43] J. Dupont, P.A.Z. Suarez, R.F. De Souza, R.A. Burrow, J.-P. Kintzinger, C–H-interactions in 1-*n*-butyl-3-methylimidazolium tetraphenylborate molten salt: solid and solution structures, *Chem. Eur. J.* 6 (2000) 2377–2381.
- [44] A. Elaiwi, P.B. Hitchcock, K.R. Seddon, N. Srinivasan, Y.-M. Tan, T. Welton, J.A. Zora, Hydrogen bonding in imidazolium salts and its implications for ambient-temperature halogenoaluminate(III) ionic liquids, *J. Chem. Soc. Dalton Trans.* 21 (1995) 3467–3472.
- [45] M. Czerwicka, S. Stolte, A. Müller, E.M. Siedlecka, M. Golebiowski, J. Kumirska, P. Stepnowski, Identification of ionic liquid breakdown products in an advanced oxidation system, *J. Hazard. Mater.* 171 (2009) 478–483.
- [46] Y. Hao, J. Peng, S. Hu, J. Li, M. Zhai, Thermal decomposition of allyl-imidazolium-based ionic liquid studied by TGA-MS analysis and DFT calculations, *Thermochim. Acta* 501 (2010) 78–83.
- [47] M.C. Kroon, W. Buijs, C.J. Peters, G.-J. Witkamp, Quantum chemical aided prediction of the thermal decomposition mechanisms and temperatures of ionic liquids, *Thermochim. Acta* 465 (2007) 40–47.